N12 Post Course Assignment

Initial Reactor Thermal Hydraulic Design

Student ID 11173631

Contents

Introduction

Nuclear technology is essential to establish colonies on the Moon and Mars. A recent comprehensive review of various potential colony sites on the Moon concluded that a colony requires 10-100 KWe of power from a nuclear reactor throughout its lifetime [1]. The Nuclear Engine for Rocket Vehicle Application (NERVA) program proved multi-GWt reactor cores for flight application with 1970s-era technology. The concept was highly successful but never flew due to financial and political troubles [2].

Considering the Vertical Landing of rockets with the SpaceX Falcon 9, a conceptual Nuclear Thermal Rocket is designed and simulated in this report. This rocket is to boost a payload from Earth orbit to Lunar orbit, then land near the prospective colony site (this report considers the Shackleton Crater) for manual reconfiguration into an electrical power plant. The 1000 MWe configuration services the potential mining and manufacturing industry alongside the colony. Reconfiguration involves plumbing changes and linking additional pump and turbine units, leaving the nuclear components untouched.

Despite the complexities of reconfiguring the reactor, the proposed concept provides several benefits over other proposed nuclear power architecture for Lunar colonies [3] [4]. The system provides three orders of magnitude more power, vastly benefiting the colony's science and communication infrastructure. The reactor is equipped with an onboard turbine and pump for thrusting in space and prospectively weighs around 15 tons with a minimum thrust-to-weight ratio greater than 2. A detailed mass analysis is out of the scope of this report. A nuclear reactor providing KWe-level power weighs around 5-10 tons [4] [5]. The proposed system has a higher weight but provides thrust, which an electrical power plant-only system cannot provide. Finally, the system can be reconfigured back into space mode at the end of life and disposed of in deep space without additional procedures.

The report organization is as follows. The next section describes the proposed system and its space and lunar configurations. The following section details the equations and assumptions used to calculate and constrain the reactor design. Then, the section after that presents the calculation results. Before the report concludes, a short section covers the reactor's operational safety. The annexure contains the code of both programs written in GNU Octave (version 7.3.0).

System Description

The proposed system has two configurations: Nuclear Thermal Rocket (NTP/Space Mode) and Nuclear Power Reactor (Power Plant/Lunar Mode). Figure 1 shows the system configuration in space mode.

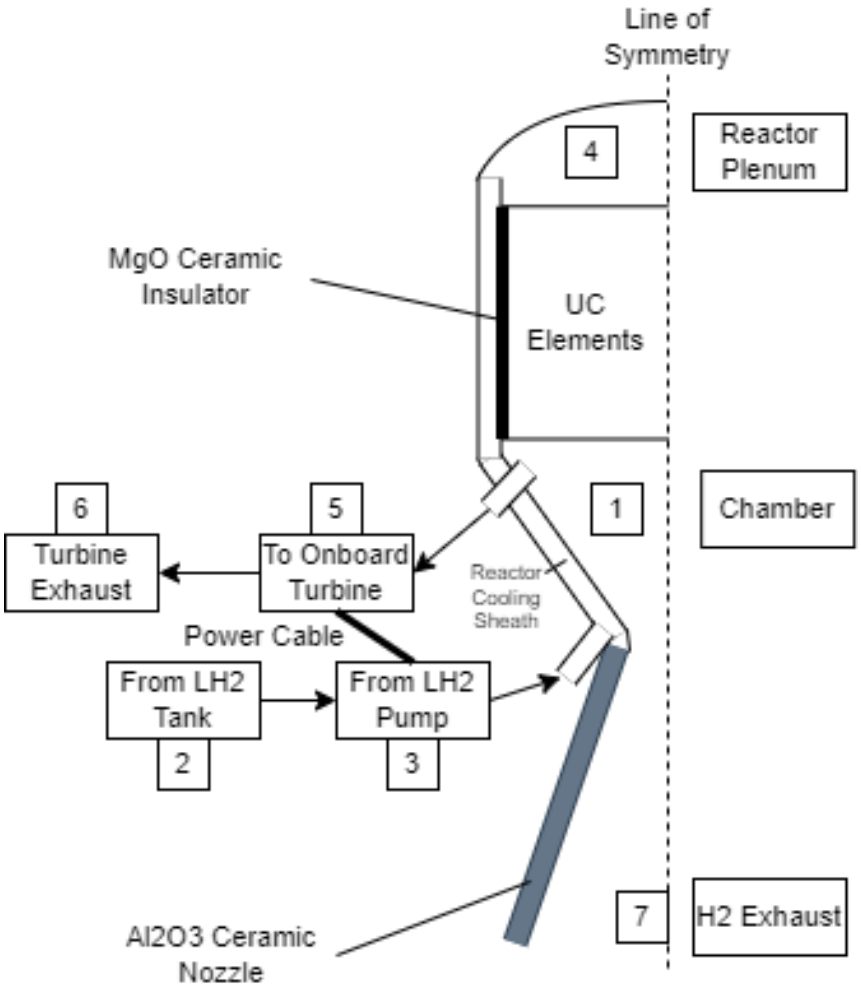

Figure 1: Reactor in Space Mode. A sequence of numbers labels the regions where the code calculates key flow parameters.

Figure 1 also shows the reactor cooling sheath which is essential for maintaining the reactor's wall temperature within permissible limits of the material during thrusting operations. The sheath also acts as a preheater, ensuring that the fluid in the reactor plenum is entirely gaseous. The ceramic nozzle decreases weight in the diverging region of the nozzle where the temperatures are not as demanding. During operation in space mode, the turbine exhausts overboard, and the calculation ignores the effects of the exhaust on thrust direction and magnitude.

After a successful deorbit from a low lunar orbit, the reactor lands on its side. Robots or colonists on the ground remove the ceramic nozzle and connect additional turbine and pump modules to the chamber outlet and sheath inlet plumbing. Figure 2 shows the configuration in lunar mode.

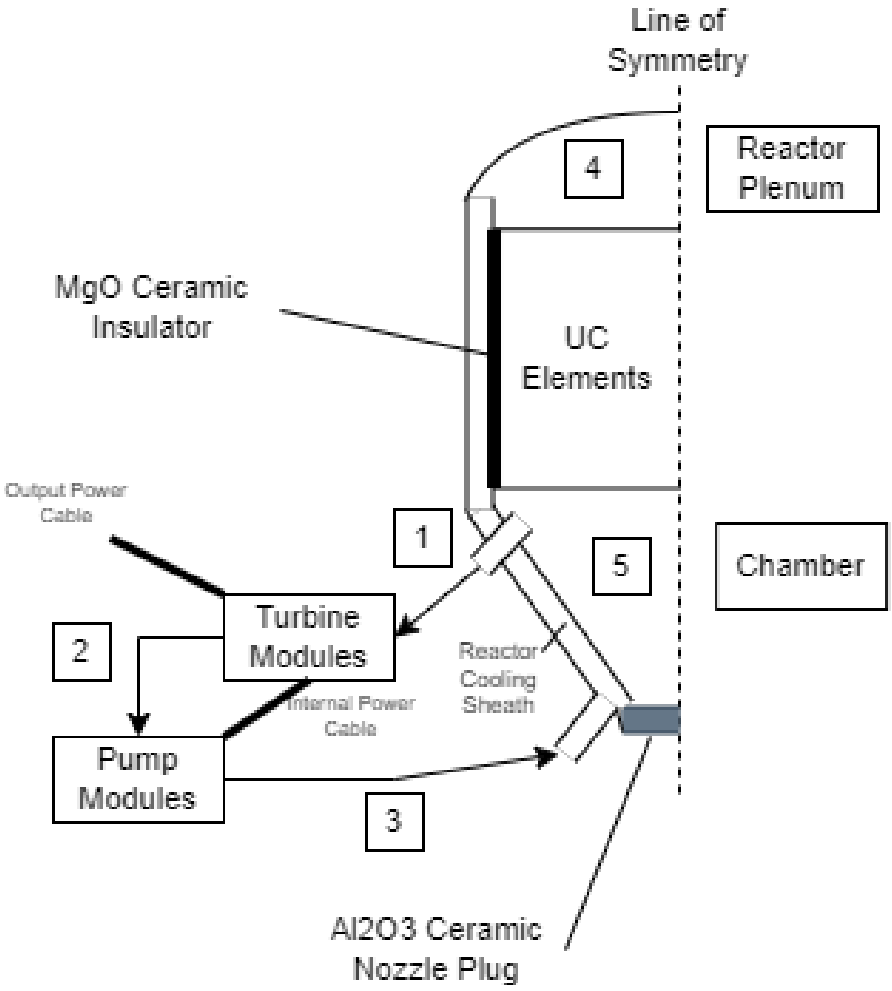

Figure 2: Reactor in Lunar Mode. A sequence of numbers labels the regions where the code calculates key flow parameters. Note the lack of any heat rejection mechanism.

The reactor in lunar mode lacks any heat rejection mechanism because there is a lack of reservoirs available on the Moon which can act as a heat sink. Usually, radiators are employed [6]. However, the calculations showed that radiators would require vast surface areas (order of 1E4 sq. mtr.) to reject significant heat, even at an ambient temperature of 70 K found in permanently shadowed regions in the Shackleton crater [1]. The radiators were inefficient because the author mandated that the reactor operates at 1373 K maximum turbine inlet temperature to ensure the use of highly reliable, low maintenance heritage uncooled turbine blade systems [7]. Additionally, operating at a significantly lower temperature limits damage to the fuel and the clad, which is essential in a reactor based on the NERVA design, which only functions for 1-2 hours of thrusting over its operational lifetime. This specific temperature value also provides benefits because it matches the materials' annealing temperature when manufactured using Spark Plasma Sintering [8]. The author posits that the annealing effect prolongs the fuel and clad lifetimes as annealing repairs damage from fission products to the crystal lattice during operation.

Reactor Materials

In the previous section, figures 1 and 2 show the extensive use of ceramics for the reactor's fuel, clad, and structural materials to minimize weight and maximize temperature resistance. Figure 3, reproduced from [9], shows the structure of a single fuel element.

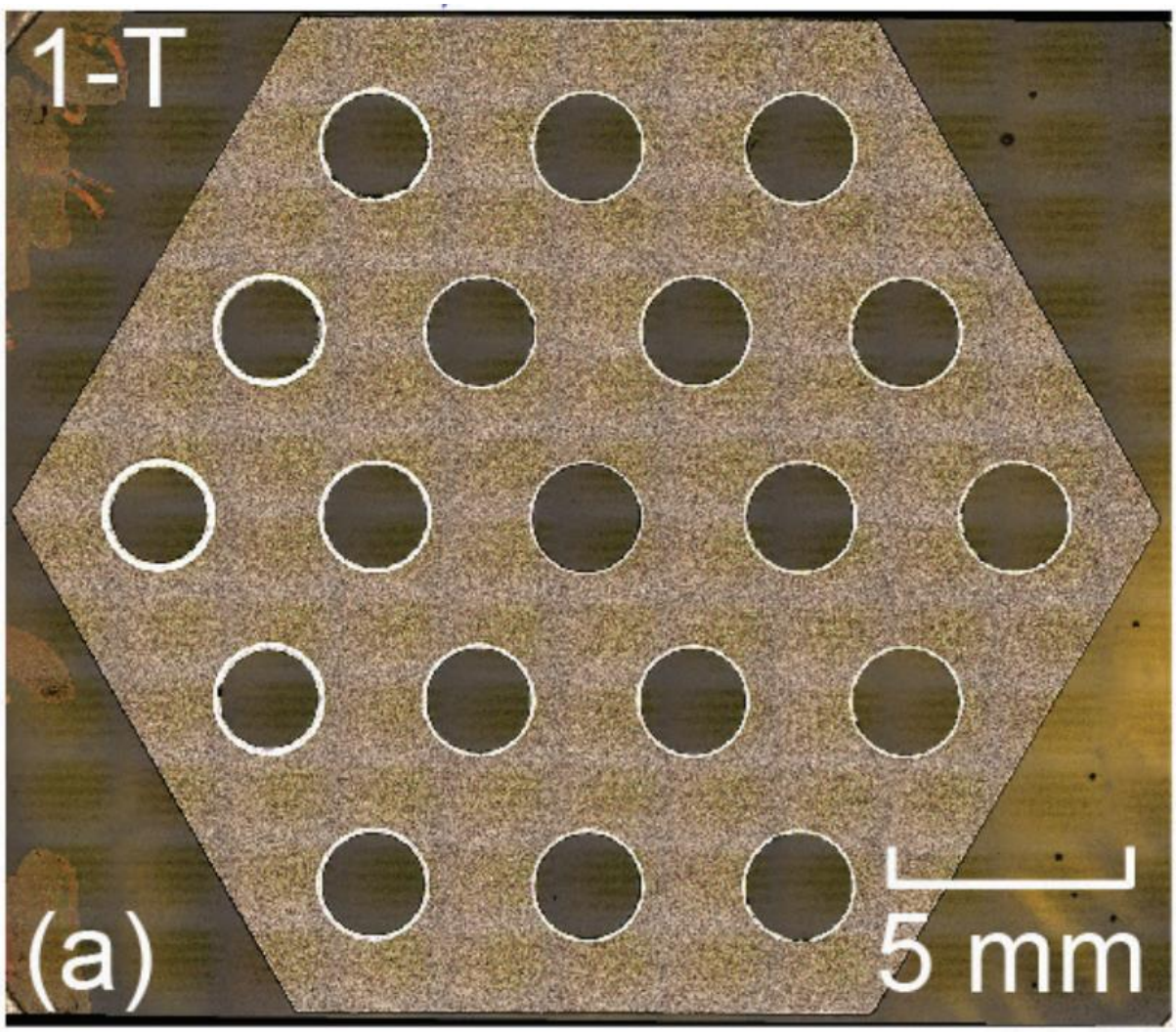

Figure 3: Cross Section of a Uranium Carbide Composite Fuel Element. Reproduced from [9]. The white rings indicate the clad, a multilayer composite in this case. The proposed fuel element uses magnesium oxide for its clad.

Table 1 shows data reproduced from [10], used to run calculations for the reactor design in this work. Stoichiometric Uranium Carbide (UC) has extensive literature studying its properties concerning fuel design [11]. Further, [12] shows that as reactor sizes and powers increase, the moderator requirements and the need to include graphite in the fuel element reduce. Thus, this reactor employs a pure UC element co-sintered with Magnesium Oxide (MgO) as a cladding material.

Table 1: Fuel Element Properties. Data reproduced from [10]. The Axial PPF and Clad Thickness are not from the references and assumed values based on information in [10].

Fuel Element Parameter	Value
No. of Coolant Channels	19
Element Power	0.65 MWt
Element Length	0.89 m
Element Radial PPF	1
Element Axial PPF	1.5
Element Width	1.905 cm
Hole Diameter	2 mm
Clad Thickness	0.25 mm
Interchannel Centre Separation	4.167 mm

After a review of ceramic claddings, the author chose **MgO** due to the following benefits. MgO has negligible neutron absorption cross-section [13]. It is naturally isotopically pure. It has a melting point of 3125 K and thermal properties compatible with UC [14]. Finally, while uranium oxides exist at reactor operating conditions, magnesium carbides do not, which means no chemical interaction between the clad and the fuel at operating temperatures. MgO is also unreactive toward hydrogen at extreme temperatures [15]. To sweeten the deal further, MgO and UC can be co-sintered using Spark Plasma Sintering in the same dye while allowing independent material properties control due to their different sintering temperatures and heating rate requirements. The sintered MgO clad is optically transparent to allow for radiative cooling of the fuel, which our calculations do not consider [16]. The disadvantages of MgO include low tensile strength and low thermal conductivity at reactor temperatures. However, the design exploits the second drawback to insulate the sheath of the reactor to prevent the wall temperatures from exceeding allowable limits.

The coolant for the system in both modes is hydrogen gas because of its high heat capacity [17] and low molecular mass. The abundance of hydrogen on the Moon is relevant because a colony usually requires onsite oxygen and hydrogen production for metal manufacturing and living environment regulation [18]. In the case of an accident, a scram and shutdown protocol shall exploit the reserve hydrogen available onsite. The reactor pressure vessel material must be hydrogen embrittlement resistant as a result. The author selects **ASTM SA-638 A-286** (UNS S66286) because of its excellent allowable stress at elevated temperatures [19] and its resistance to hydrogen embrittlement [20]. The author investigated oxygen gas as a coolant but found that huge flow rates are required to extract heat from the reactor core in the 1000 MWe scenario.

Finally, an aluminium oxide nozzle skirt overcomes the corrosion problems of graphite and its composites, usually used in radiatively cooled nozzles [21], in a hot hydrogen environment [2] [9] because aluminium oxide is resistant to high-temperature hydrogen [22]. MgO has a higher working temperature, but aluminium oxide is mechanically more robust and easier to manufacture [23]. It also has high black body emissivity in the infrared region, simplifying the skirt's design [24].

Calculation Methodology

The calculation procedure for the space mode reactor proceeds as follows. The code must determine the flow variables of pressure, mass flow, flow area and temperature at each labelled point in Figure 1. We omit the shielding and reflector cooling because the calculation required detailed neutronic calculations to find the heat deposition, which is out of the scope of this report. The code input comprises the estimated flow variables at point 1, material temperature limits and pressure vessel safety factors. At point 2, the liquid hydrogen tank holds liquid hydrogen at 20 K and 2.25 atm, the same as the NASA Space Shuttle External Tank [25]. The pump outputs fluid at **5 MPa** in all operation configurations and modes. The code uses hydrogen properties throughout the calculation at the 5 MPa isobar provided in [17]. The code ignores changes in material properties with pressure, except for density, because data in [17] shows minimal variation between the 4-5 MPa isobars.

The pump uses an upscaled version of the electric motor design presented in [26]. A similar motor converts the mechanical energy into electricity in the turbine. Note that the turbomachines are not mechanically connected, simplifying the electrical power architecture at the expense of energy conversion loss. The system turbomachinery comprises a three-stage turbine and three-stage pump, each with a stage pressure ratio of 1.61 [12]. However, the motor efficiencies are around 0.9, leading to a fair tradeoff [26]. The author notes that the fluid is in its supercritical phase throughout the system, and no boiling occurs [27]. The code employs isentropic relations presented in [21] for determining the reactor and nozzle area rations and hence, the geometry.

The pump power input, assuming no change in density and temperature across the pump, is given as

$$P_{Pmp} = \eta_{motor}^{-1} \eta_{machine}^{-1} \nu_{H_2}(5\,MPa, 20K)\, \dot{m}\, (P_{out} - P_{tank})$$

Here, 0.9 and 0.7258 are the electrical and mechanical efficiencies [12], respectively. The other symbols have their usual meaning.

In the lunar mode, the input to the pump is a gas. Hence, the following compressible work equation from [28] yields the compressor power

$$P_{Comp} = \eta_{motor}^{-1} \eta_{machine}^{-1} \dot{m}\, c_p(T_{in})\, T_{in} \left(\left(\frac{P_{out}}{P_{in}} \right)^{\frac{\gamma-1}{\gamma}} - 1 \right)$$

The electrical and mechanical efficiencies are assumed to be the same as for the pump. Here, gamma stands for the gas ratio of heat capacities which is 1.4 for ideal diatomic gases. The assumption of ideal gas shows appreciable error only in the region of 20 to 100 K, which is negligible compared to the fluid temperature range from 20 K to 2800 K.

The equation below describes the turbine power output in all configurations.

$$P_{Turb} = \eta_{motor}\,\eta_{machine}\,\dot{m}\,C_p(T_{in})\,T_{in}\left(1-\left(\frac{P_{out}}{P_{in}}\right)^{\frac{\gamma-1}{\gamma}}\right)$$

The efficiencies of the electrical and mechanical components are 0.9 and 0.7171 [12], respectively. The other symbols have their usual meaning.

The neutron flux profile dictates the temperature profile in the reactor. For this calculation, the author assumes a chopped cosine profile with an axial power peak of 1.5. While the peaking factor in the literature is 1.67 [10], the mathematical structure of the profile function does not allow peaks greater than 1.57.

$$q_i = \frac{0.65E6}{19}\cos\left(\frac{\pi z_i}{H_{ex}}\right)\Delta z \quad , \quad H_e = 0.89\,m \quad , \quad H_{ex} = 0.93463\,m$$

Hence, the code uses a value of 1.5 with an extrapolated element length of 0.93463 m. The other peaking factors for a NERVA-type reactor are very close to 1 because the fuel loading changes can compensate for the power concentration [10]. The fuel elements are 93% enriched uranium-235 UC [10]. The reactor reduces the per-element power to scale the output for the 1000 MWe lunar mode configuration.

Figure 4 shows coolant channels in the fuel element. The primary unit cell of the lattice is a triangle with a side length of the interchannel centre separation. The red region depicts the MgO clad, the blue region shows the coolant bulk, and the grey region is the surrounding UC.

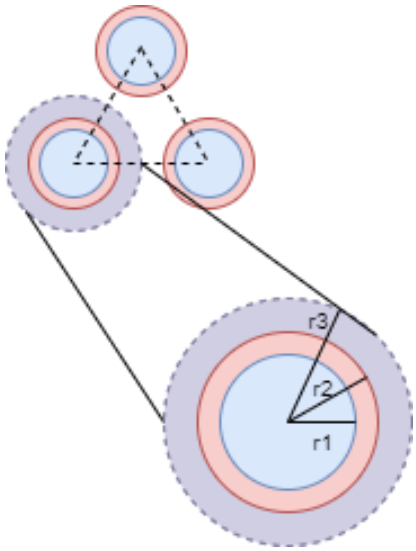

Figure 4: Schematic of Coolant Channels in Fuel Element

The equations below describe the reactor temperature profile at the i^{th} vertical slice with the centre of the fuel element as the reference.

$$T_{b,i+1} = T_{b,i} + \left[\dot{m}\, C_p(T_{b,i})\right]^{-1} q_i$$

$$HTC(T_{b,i}, T_{c,i}) = \frac{K(T_{b,i})}{D_h} \times 0.205 \times Re(T_{b,i})^{0.8} \times Pr(T_{b,i})^{0.4} \times \left[\frac{T_{c,i}}{T_{b,i}}\right]^{-0.55}$$

$$T_{c,i} = T_{b,i} + \frac{q_i}{2\pi r_1 \Delta z\, HTC([T_{b,i}, T_{c,i})}$$

$$T_{s,i} = T_{c,i} + \frac{q_i}{2\pi \Delta z\, K_c(T_{c,i})} \times \ln\left(\frac{r_1}{r_2}\right)$$

$$T_{m,i} = T_{s,i} + \frac{q_i}{\Delta z}\left[\frac{1}{4\pi K_g(T_{s,i})} + \ln\left(\frac{r_3}{r_2}\right) \times \left[\frac{1}{2\pi K_c(T_{s,i})} + \frac{r_2^2}{2\pi K_g(T_{s,i})(r_3^2 - r_2^2)}\right]\right]$$

[29] describes the heat transfer coefficient model for the fluid-clad interface for hydrogen-cooled reactors in NTP systems. The derivation of these equations is available from the author on request. The symbols have their usual meaning. The functions for cladding and fuel thermal conductivity are available in [11] and [30], respectively. However, they are valid for the range of 200 K to the respective melting points of the materials. The code extrapolates the conductivity data in a physically reasonable manner when the fluid is below 200 K. This extrapolation only occurs in the first couple of centimetres of the fuel element and induces very little error in the overall temperature profile.

Next, we describe the pressure losses in the system. The code systematically neglects form losses and external plumbing losses because a detailed plumbing design is out of the scope of this report.

$$Re(T) = \frac{\rho v D_h}{\eta(T)} = \frac{\dot{m} D_h}{A \eta(T)} = \frac{2\dot{m}}{\pi (r_1 + r_2) \eta(T)} \quad \because D_h = \frac{4A}{S_w}$$

$$\left[\frac{dP}{dx}\right]_{friction} = \frac{f(Re)\,\Delta x}{2\rho(T) D_h}\left[\frac{\dot{m}}{A}\right]^2$$

$$\left[\frac{dP}{dx}\right]_{acc} = \frac{\dot{m}}{A}\frac{dU}{dx} \; ; \; \Delta P_{acc} = \dot{m} \int_{U_{in}}^{U_{out}} \frac{dU}{A(U)} = \left[\frac{\dot{m}}{A}\right]^2 \left[\frac{1}{\rho_{out}} - \frac{1}{\rho_{in}}\right]$$

If A is constant

The calculation modifies the standard definition of the Reynolds number to account for flow in annular geometries, treating the circular channel as a particular case with one radius set to 0. The modification simplifies computations in the reactor cooling sheath. The author draws the reader's attention to the above expression of frictional pressure loss. Due to extremely high Reynolds numbers in the coolant channels, the value of the Darcy factor, defined by the equation below, is minuscule.

$$f(Re) = \begin{cases} 64/Re, & Re < 3000 \\ 0.316\, Re^{-0.25}, & 3000 < Re < 30000 \\ 0.184\, Re^{-0.2}, & Re > 30000 \end{cases}$$

An order of magnitude analysis reveals that the order of pressure loss in this mode is 1E3. In practice, the code computes losses anywhere between 157 to 530 Pa. The magnitude of pressure loss is negligible compared to the operating pressure of 5 MPa. Gravitational pressure losses do not exist when the reactor is thrusting in space and are negligible in lunar mode due to the low gravity on the Moon and the low density of the coolant. Thus, acceleration losses are the only significant loss mode explored in this report. However, the change in flow area is complicated to express as a function of the flow velocity. The code assumes the flow area to be constant at the minimum area encountered by the flow across the component in question while calculating the pressure change to obtain worst-case values.

The changes in fluid properties as it passes through the reactor cooling sheath are critical to quantify. The equations below list two methods to calculate the heat flux into the sheath. The first method assumes the worst-case temperature gradient, and that conductive transfer dominates. The second method [31] assumes that convective transfer dominates with the worst-case temperature gradient. Both cases yield similar values of the order of 1E6 W. The conduction model is equally applicable for both reactor configurations, whereas no significant convective transfer is possible if there is no nozzle flow.

$$Q_{rgen\ (Conductive)} = K A \frac{(T_{flow} - T_{wall})}{t_{PV}} \simeq K A \frac{T_{flow}}{t_{PV}}$$

$$Q_{rgen\ (Bartz)} = \iint_{Surf} \left[\frac{K_f}{D_h} \times 0.026 \times Re^{0.8} \times Pr^{0.4} \right] (T_{flow} - T_{wall})\, dA$$

Calculating the convective model is complicated because the variables are functions of positions or temperature. Hence, **the author highlights the simplicity of the conduction model in providing reasonable engineering estimates**. The code calculates both values and selects whichever is the higher one. It then solves the following integral equation to find the sheath outlet temperature.

$$T_{rgen\ (Outlet)} \Leftarrow \int_{T_{min}}^{T_{rgen(Out)}} \dot{m}\, c_p(T)\, dT - \int_{T_{min}}^{T_{rgen(In)}} \dot{m}\, c_p(T)\, dT = Q_{rgen}$$

A similar equation can determine the compressor or turbine outlet temperature. The minimum possible fluid temperature in the loop provides a reference for the integrals to compute the change in flow enthalpy.

$$T_{out} \Leftarrow \int_{T_{min}}^{T_{out}} \dot{m}\, c_p(T)\, dT - \int_{T_{min}}^{T_{in}} \dot{m}\, c_p(T)\, dT = P_{machine}$$

Finally, the code finds the theoretical and actual Brayton cycle efficiencies.

$$\eta_{th} = 1 - \frac{T_{min,\,loop}}{T_{Chamber}}$$

Calculation Results

The code uses equations and data presented in the previous sections to calculate reactor and flow parameters at various points in the system. Two programs run calculations. The first program determines the system in space mode. The second program uses the output of the first program to determine the flow parameters for the 1000 MWe power plant configuration. This report investigates the effect of changing reactor power on the output parameters from a reactor power of 2.75 GWt to 2 GWt to ensure the 1000 MWe scenario is possible, considering a maximum conversion efficiency of around 0.5. Table 2 shows the outputs of the first program. The chamber bypass factor is 0.0065 for all reactors.

Table 2: Variation of Reactor Parameters with Reactor Thermal Power

Parameter	**2 GWt Reactor**	**2.25 GWt Reactor**	**2.5 GWt Reactor**	**2.75 GWt Reactor**
Minimum Chamber Pressure	4.7344E6 Pa	4.7338E6 Pa	4.7326E6 Pa	4.7336E6 Pa
Chamber Temperature	2638.2 K	2642.0 K	2630.5 K	2636.9 K
Minimum Mass Flow Rate	28.5 Kg / s	32 Kg / s	35.75 Kg / s	39.2 Kg / s
Mass of UC	1.1978E4 Kg	1.3476E4 Kg	1.4974E4 Kg	1.6468E4 Kg
Vessel Radius	0.5939 m	0.6299 m	0.6640 m	0.6963 m
Thrust	2.3964E5 N	2.6926E5 N	3.0016E5 N	3.2953E5 N
ISP in Vacuum	862.82 s	863.44 s	861.56 s	862.6 s
Theoretical Efficiency	0.6541	0.6546	0.6531	0.6540

As seen in Table 2, the 2.25 GWt offers the least weight and mass flow rate at the highest efficiency. Figure 5 shows the entire output of the first program for this reactor configuration. The right-hand side of the image provides a guide to what the output variables on the left-hand side represent. The total number of fuel elements in the reactor is 3462. The turbine receives only 0.65 % of the pump output mass flow because, in space mode, the reactor only produces power to run the pump and some peripheral electronics. The low net power output causes the calculated actual thermal efficiency to be anomalously low. A separate line from the liquid hydrogen tank feeds the turbine inlet with the chamber bypass to ensure the overall turbine inlet temperature stays at 1373 K.

Figure 5: Program One Output for the Selected 2.25 GWt Reactor

Figures 6 and 7 show the variation of power and temperature along any given fuel element in the 2.25 GWt reactor.

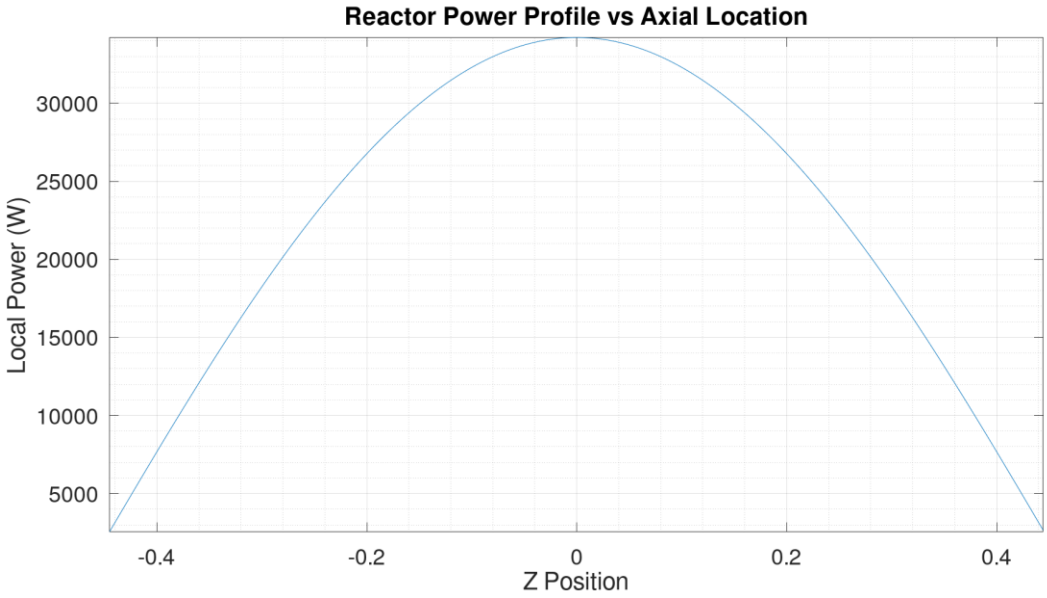

Figure 6: 2.25 GWt Reactor Power Profile vs Axial Location in Meters

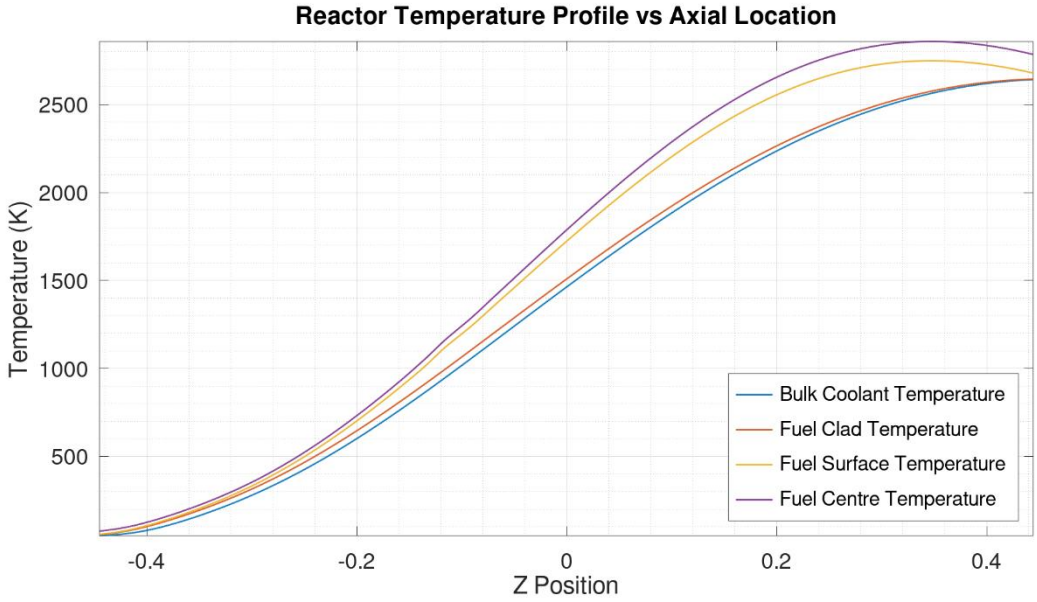

Figure 7: 2.25 GWt Reactor Temperature Profiles vs Axial Location in Meters

Figure 6 clearly shows the chopped cosine flux profile. Figure 7 and data in Figure 5 show the characteristic drop in fuel temperatures after the element midpoint expected from a chopped cosine power profile. These results verify the qualitative accuracy of the calculations.

The second program uses the outputs shown in Figure 5 to calculate the reactor parameters in the lunar mode for the 1000 MWe scenario. Table 3 summarizes the output of the code.

Parameter	Value
Thermal Output	1.82 GWt
Electrical Output	1.0822 GWe
Actual Thermal Efficiency	0.5946
Theoretical Thermal Efficiency	0.6024
Total Turbine Power	1.5361 GWe
Total Compressor Power	453.92 MWe
Compressor Stage Pressure Ratio	2.6837
Chamber Temperature	1372.8 K
Chamber Pressure	4.5053 MPa

Figure 8 shows the entire output of the second code for the 1000 MWe scenario. The configuration achieves actual efficiencies close to the 0.60 theoretical value.

Figure 8: Program Two Output for the Selected Reactor Reconfigured for Lunar Surface Power Generation

Brief Review of System Safety

The NERVA program extensively tested the concepts on which the reactor proposed here is based on [2]. The program did not consider the environmental effects of fission products in the exhaust. The MgO clad overcomes the issues of cracking, and corrosion in the zirconium carbide clad [9]. Thus, the current design should contain less radioactivity in its exhaust.

Further, contamination concerns are low due to the ceramic nature of its fuel. If submerged in seawater or wet sand, the criticality safety review of the legacy reactor suggests that it would not go critical [32]. The triply redundant control system of anti-criticality poison system, reflector drum and hydrogen moderation offer tight control of the reactivity of the fuel [33]. During nominal operation, the control drum or reflector, made of beryllium oxide, controls the fuel reactivity. In accident situations, control rods control and scram the reactor. The reactor has a negative power coefficient of reactivity power due to the moderating nature of hydrogen and significant density changes during a thermal excursion.

In the lunar mode, the proposed configuration provides significant amounts of power while providing thrust to boost the payload to the Moon. Such a system is critical for establishing a colony or industrial site on the Moon. Future dedicated architecture is more suited for a longer-term power supply. At the end of life (70 years), the burnup of uranium in the reactor is about 3 % [3]. However, at its heart, the reactor is based on technology designed to operate for 1-2 hours, and lunar colonists can not expect a 70-year lifespan. In any case, the system simplifies radioactive waste disposal as the reactor is reconfigured for flight at the end of life and launched from the site into deep space. For security purposes, to prevent the repurposing of the reactor or its fuel, it is instructed to melt down at the end of the final burn.

The loss of coolant or power conversion machinery during operation is also covered. As mentioned, a lunar colony requires onsite hydrogen gas storage for various essential roles. In the event of a total loss of coolant, the reactor safely scrams itself with minimal damage to the fuel elements [33]. The decay heat removal process utilizes the colonies' reserve hydrogen for a graceful shutdown. In both lunar mode configurations, multiple turbine and compressor modules are available in case of failure. If a turbine module fails, the operator ramps down the compressors and gracefully shuts down the reactor. If a compressor module fails, the operator reduces the reactor's power to compensate for the lower net coolant mass flow until the reactor scrams.

Conclusion

This report explored the design of a nuclear propulsion system repurposable for power generation after the system lands on the lunar surface. It covers the advantages of such a system over sending a nuclear power plant to the Moon.

The work discusses the materials required for reactor construction. The fuel elements use 93 % enriched uranium 235 as a stoichiometry carbide with a clad of co-sintered transparent magnesium oxide. The coolant is hydrogen gas to reduce flow rates and increase thrusting performance.

The work also presents detailed equations and calculations to determine the reactor geometry and flow parameters. It makes vital assumptions to simplify pressure loss calculations. The calculations show that a 2.25 GWt reactor provides the best thrusting performance. The second program uses this reactor to find the performance of a power plant reconfigured from that reactor code for producing 1000 MWe on the Moon's surface. Finally, the report includes a brief review of the reactors' operational safety in various scenarios.

Bibliography

[1] M. Kaczmarzyk and M. Musiał, "Parametric study of a lunar base power systems," *Energies,* vol. 14, p. 1141, 2021.

[2] W. Robbins, "An historical perspective of the NERVA nuclear rocket engine technology program," in *Conference on Advanced SEI Technologies*, 1991.

[3] M. S. El-Genk and T. M. Schriener, "Long operation life reactor for lunar surface power," *Nuclear engineering and design,* vol. 241, p. 2339–2352, 2011.

[4] J. O. Elliott, K. Reh and D. MacPherson, "Lunar fission surface power system design and implementation concept," in *AIP Conference Proceedings*, 2006.

[5] A. Pizarro-Chong, C. Wang, C. Ma and L. Zhang, "Development of space nuclear reactors for lunar purposes: Overview of technical and non-technical issues," in *2010 3rd International Symposium on Systems and Control in Aeronautics and Astronautics*, 2010.

[6] A. Mazzetti, M. G. Pret, G. Pinarello, L. Celotti, M. Piskacev and A. Cowley, "Heat to electricity conversion systems for moon exploration scenarios: A review of space and ground technologies," *Acta Astronautica,* vol. 156, p. 162–186, 2019.

[7] U. Unnikrishnan and V. Yang, "A review of cooling technologies for high temperature rotating components in gas turbine," *Propulsion and Power Research,* 2022.

[8] D. Salvato, J.-F. Vigier, M. Cologna, L. Luzzi, J. Somers and V. Tyrpekl, "Spark plasma sintering of fine uranium carbide powder," *Ceramics International,* vol. 43, p. 866–869, 2017.

[9] S. V. Raj and J. A. Nesbitt, "Development of Advanced Coatings for NERVA-type Fuel Elements," *NETS2015-5072, Nuclear and Emerging Technologies for Space (NETS),* 2015.

[10] S. K. Borowski, R. J. Sefcik, J. E. Fittje, D. R. McCurdy, A. L. Qualls, B. G. Schnitzler, J. Werner, A. Weitzberg and C. R. Joyner, "Affordable development and demonstration of a small NTR engine and stage: how small is big enough?," in *AIAA SPACE 2015 Conference and Exposition*, 2015.

[11] G. Vasudevamurthy and A. T. Nelson, "Uranium carbide properties for advanced fuel modeling–A review," *Journal of Nuclear Materials,* vol. 558, p. 153145, 2022.

[12] *Near-term nuclear propulsion FY92 Final Review - NASA,* NASA, 1992.

[13] J. Kopecky, *Atlas of Neutron Capture Cross Sections,* IAEA, 2014.

[14] G. Himpel, M. Herrmann and S. Höhn, "Comparison of the high-temperature corrosion of aluminium nitride, alumina, magnesia and zirconia ceramics by coal ashes," *Ceramics International,* vol. 41, p. 8288–8298, 2015.

[15] H. Kobayashi, M. Yamaguchi and T. Ito, “Ab initio MO study on adsorption of a hydrogen molecule onto magnesium oxide (100) surface,” *Journal of physical chemistry,* vol. 94, p. 7206–7213, 1990.

[16] X. Chen and Y. Wu, “Fabrication and optical properties of highly transparent MgO ceramics by spark plasma sintering,” *Scripta Materialia,* vol. 162, p. 14–17, 2019.

[17] R. D. McCarty, *Selected Properties of Hydrogen (Engineering Design Data),* NIST Technical Series Publications, 1981.

[18] *Hydrogen,* 2021.

[19] *Maximum Allowable Stress Values S for Ferrous Materials according to ASME Code Section II, Part D, Table 1A, 2021 Edition,* American Society of Mechanical Engineers, 2021.

[20] W. T. Chandler, “Hydrogen embrittlement and its control in hydrogen-fueled engine systems,” *NASA. Langley Res. Center Recent Advan. in Structures for Hypersonic Flight, Pt. 1,,* 1978.

[21] G. P. Sutton and O. Biblarz, Rocket propulsion elements, John Wiley & Sons, 2016.

[22] S. W. Weller and A. A. Montagna, “Studies of alumina I. Reaction with hydrogen at elevated temperatures,” *Journal of Catalysis,* vol. 21, p. 303–311, 1971.

[23] B.-N. Kim, K. Hiraga, K. Morita and H. Yoshida, “Spark plasma sintering of transparent alumina,” *Scripta Materialia,* vol. 57, p. 607–610, 2007.

[24] V. Sarou-Kanian, J.-C. Rifflet and F. Millot, “IR radiative properties of solid and liquid alumina: Effects of temperature and gaseous environment,” *International Journal of Thermophysics,* vol. 26, p. 1263–1275, 2005.

[25] *Space Shuttle External Tank,* Wikimedia Foundation, 2022.

[26] J. S. Smith, A. P. Watson and others, “Design, Manufacture, And Testing Of A High Speed 10 MW Permanent Magnet Motor And Discussion Of Potential Applications.,” in *Proceedings of the 35th Turbomachinery Symposium*, 2006.

[27] Z. Han, J. Zhang, M. Wang, W. Tian, S. Qiu and G. H. Su, “A modified system analysis code for thermo-hydraulic calculation of hydrogen in a nuclear thermal propulsion (NTP) system,” *Annals of Nuclear Energy,* vol. 164, p. 108632, 2021.

[28] *Compressor,* Wikimedia Foundation, 2022.

[29] F. A. Campi, J. W. H. Chi, E. A. De Zubay, J. D. Holmgren and A. M. Vetere, “Transient two-phase heat transfer and flow characteristics of liquid hydrogen,” 1963.

[30] A. M. Hofmeister, “Thermal diffusivity and thermal conductivity of single-crystal MgO and Al2O3 and related compounds as a function of temperature,” *Physics and Chemistry of Minerals,* vol. 41, p. 361–371, 2014.

[31] D. R. Bartz, “Turbulent boundary-layer heat transfer from rapidly accelerating flow of rocket combustion gases and of heated air,” in *Advances in Heat Transfer*, vol. 2, Elsevier, 1965, p. 1–108.

[32] G. Farbman, “Upgraded NERVA systems: Enabler nuclear system,” in *NASA. Lewis Research Center, Nuclear Thermal Propulsion: A Joint NASA (DOE) DOD Workshop*, 1991.

[33] *NERVA Program Summary Report No. 6 (1967),* NASA, 1967.

[34] *Compressor,* Wikimedia Foundation, 2022.

Annexure

The above object contains the code of the first GNU Octave program that calculates the reactor flow parameters and geometry.

The above object contains the second GNU Octave program code that calculates the reactor flow parameters and geometry.